Vibrational properties of graphene nanoribbons by first-principles calculations

Roland Gillen, Marcel Mohr, Christian Thomsen, and Janina Maultzsch
Institut für Festkörperphysik, Technische Universität Berlin, Hardenbergstr. 36, 10623 Berlin, Germany
(Received 13 February 2009; revised manuscript received 14 July 2009; published 6 October 2009)

We investigated the vibrational properties of graphene nanoribbons by means of first-principles calculations on the basis of density-functional theory. We confirm that the phonon modes of graphene nanoribbons with armchair- and zigzag-type edges can be interpreted as fundamental oscillations and their overtones. These show a characteristic dependence on the nanoribbon width. Furthermore, we demonstrate that a mapping of the calculated Γ-point phonon frequencies of nanoribbons onto the phonon dispersion of graphene corresponds to an "unfolding" of nanoribbons' Brillouin zone onto that of graphene. We consider the influence of spin states with respect to the phonon spectra of zigzag nanoribbons and provide comparisons of our results with past studies.

DOI: 10.1103/PhysRevB.80.155418 PACS number(s): 61.48.De, 63.22.−m, 63.20.dk

I. INTRODUCTION

The outstanding properties of graphene and graphene-related structures of nanosize gave rise to extensive theoretical and experimental researches during the last two decades. Along with the heavily studied carbon nanotubes (CNTs) another quasi-one-dimensional (1D) nanostructure aroused special interest: terminated stripes of graphene, so-called graphene nanoribbons (GNRs). Recent progress in preparation of single-layered graphene sheets[1–4] allows the fabrication of GNRs through lithographic[5] techniques, chemical dissolving from bulk graphite,[6] and, most recently, the fabrication of nanoribbons by cutting suitable nanotubes,[7–9] and thus possibly the verification of theoretical predictions regarding electronic and optical properties. In the course of such investigations interesting magnetic and electronic properties,[10–17] quasirelativistic behavior of electrons and the possibility of band-gap engineering[5,18–20] by varying ribbon widths were shown. These results make GNRs seem promising for future developments in nanotechnology and nanoelectronics. The propagation of valence electrons in graphene structures is accompanied by exceptionally strong electron-phonon coupling.[21] The investigation of the vibrational spectrum in these materials is thus of fundamental importance for the electron transport in electronic devices and of great general interest.

In this paper, we present our studies of the Γ-point phonons of different armchair and zigzag nanoribbons, obtained through *ab initio* density-functional theory (DFT) calculations. We found that it is possible to classify the Γ-point phonon modes of hydrogen passivated GNRs into fundamental oscillations, overtones, and C-H vibrational modes. Fundamental oscillations and overtones can be mapped onto the graphene phonon dispersion by unfolding the GNR Brillouin zone onto that of graphene. Furthermore, we discuss the dependence of GNR phonon frequencies on the nanoribbon width.

II. CALCULATIONS

Graphene nanoribbons can, at least in some cases, be understood as cut and unrolled carbon nanotubes. These geometric similarities suggest that the phonon spectra of comparable CNTs and GNRs may be similar. On the other hand, unlike CNTs, nanoribbons possess edges, which have a lower coordination number and technically, they require special treatment. A widespread method to take care of the carbon atoms at the edges in calculations is to passivate the dangling bonds with single atoms or molecules, mainly hydrogen, in order to sustain the bonding structure in graphene, i.e., the aromaticity and the sp^2 hybridization of the carbon atoms. Because the diversity in the possibilities to cut out GNRs of a graphene sheet is larger than to "roll" it into a seamless cylinder, i.e., carbon nanotubes, the number of edge types is very large. In this paper, however, we will only consider nanoribbons with pure armchair- or zigzag-typed edges, which can be calculated with reasonable computional cost and are a good starting point for costly research on nanoribbons with mixed-type edges. There are various approaches for the classification of armchair graphene nanoribbons (AGNRs) and zigzag nanoribbons (ZGNRs). Some approaches use a (p,q) (Ref. 18) type classification with two characteristic integers, similar to the common classification of CNTs, or a classification that is based on the number of honeycombs along the ribbon width.[22] For the purpose of this paper entirely sufficient is the approach of Fujita *et al.*,[10] where GNR are classified by their edge type into AGNR and ZGNR, and giving the number of dimers N in the unit cell (see Fig. 1). The unit cell with N dimers is extended periodically along the z direction, resulting in an infinitely long strip of graphene.

We define the width of a graphene nanoribbon as the distance between the central points of the outmost dimers (refer to Fig. 1). The ideal ribbon width, i.e., the width of an unrelaxed nanoribbon, is dependent on N and given by

$$w_{\mathrm{AGNR}} = \frac{1}{2}(N-1)a_0 \tag{1}$$

and

$$w_{\mathrm{ZGNR}} = \frac{\sqrt{3}}{2}(N-1)a_0 \tag{2}$$

with the graphene lattice constant a_0. In our calculations, the lattice constant of a relaxed sheet of graphene is a_0

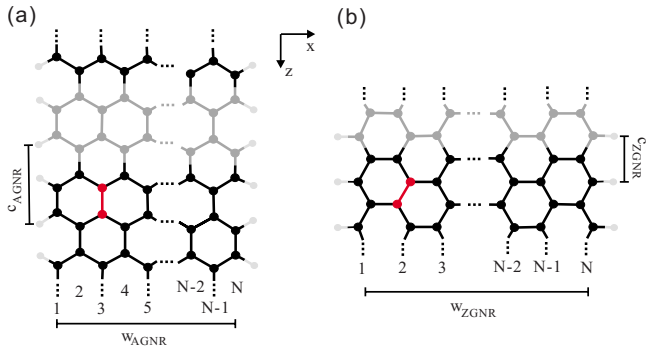

FIG. 1. (Color online) Structure of (a) a N-AGNR and (b) a N-ZGNR. In each case one dimer is emphasized in dark gray (red) and a unit cell is emphasized in gray, respectively. The ideal lattice constants of the nanoribbons are $c_{AGNR}=\sqrt{3}a_0$ and $c_{ZGNR}=a_0$. The corresponding ideal ribbon widths, i.e., the distance between C atoms at opposing edges, are given by Eqs. (1) and (2), respectively.

$=2.4656$ Å. The width of N-ZGNRs with odd N is equivalent to the circumference of an $(\frac{N-1}{2},\frac{N-1}{2})$ CNT. Thus, these nanoribbons could be rolled into armchair nanotubes. For N-ZGNR with even N, however, there are no corresponding nanotubes. Similarly, the width of N-AGNRs with odd N is equivalent to the chiral vector of a $(\frac{N-1}{2},0)$ CNT, whereas AGNRs with even N do not correspond to any nanotube. The relaxation, however, results in nanoribbon widths slightly below (for AGNRs) or above (for ZGNRs) the values calculated with these equations (see Tables I and II). These deviations decrease with increasing ribbon width.

We used density-functional theory in the local approximation form[23] to calculate N-AGNRs and M-ZGNRs with the number of dimers per unit cell $N=7\cdots15$ and $M=3\cdots14$, respectively. Pseudopotentials were generated with the Troullier-Martins scheme[24] for the following valence-state configurations: C $2s^2(1.49),2p^2(1.50)$; H $1s^1(1.25)$, where

TABLE I. Lattice constants c and widths w of various relaxed zigzag-edged graphene nanoribbons. $\Delta=\frac{c-c_{ideal}}{c_{ideal}}$ is the relative deviation of the calculated lattice constant from the ideal lattice constant $c_{ideal}=2.4656$ Å. The ideal width was calculated by Eq. (1).

N	c (Å)	Δ (%)	w (Å)	w_{ideal} (Å)
2	2.461877	−0.15	2.141	2.135
3	2.461083	−0.18	4.286	4.27
4	2.461787	−0.15	6.427	6.406
5	2.462023	−0.14	8.566	8.541
6	2.46277	−0.11	10.702	10.676
7	2.465000	−0.02	12.838	12.811
8	2.46414	−0.06	14.975	14.947
9	2.464095	−0.06	17.113	17.082
10	2.464095	−0.06	19.249	19.217
12	2.464195	−0.06	23.523	23.488
14	2.464649	−0.04	27.794	27.758
16	2.464730	−0.04	32.067	32.029

TABLE II. Lattice constants c and widths w of various relaxed armchair-type graphene nanoribbons. $\Delta=\frac{c-c_{ideal}}{c_{ideal}}$ is the relative deviation of the calculated lattice constant from the ideal lattice constant $c_{ideal}=\sqrt{3}a_0=4.27$ Å. The ideal width was calculated by Eq. (1).

N	c (Å)	Δ (%)	w (Å)	w_{ideal} (Å)
4	4.318	1.1	3.653	3.698
5	4.309	0.9	4.885	4.931
6	4.308	0.9	6.107	6.164
7	4.296	0.6	7.353	7.3968
8	4.293	0.5	8.587	8.629
9	4.294	0.5	9.809	9.862
10	4.289	0.4	11.056	11.095
11	4.288	0.4	12.185	12.328
12	4.288	0.4	13.511	13.561
13	4.287	0.4	14.753	14.794
14	4.284	0.3	15.988	16.026
15	4.284	0.3	17.212	17.259
16	4.284	0.3	18.454	18.492
17	4.284	0.3	19.689	19.725
20	4.28	0.2	23.381	23.423
21	4.28	0.2	24.609	24.656
22	4.28	0.2	25.846	25.889

the value in parenthesis indicates the pseudopotential core radii in bohr. The valence electrons were described by a double-ζ basis set plus an additional polarizing orbital. The localization of the basis followed the standard split scheme and was controlled by an internal SIESTA (Refs. 25 and 26) parameter, the energy shift, for which a value of 50 meV was used. This resulted in basis functions with a maximal extension of 3.31 Å (C) and 3.2 Å (H). As SIESTA works with periodic boundary conditions, the lattice vectors in direction perpendicular to the nanoribbon axis were scaled in such a way that the space between periodic images of the nanoribbons was at least 20 Å in order to prevent interaction between them. Real-space integrations were performed on a grid with a fineness of 0.08 Å, which can represent plane waves up to an energy of 270 Ry.

A minimum of 30 k points equally spaced along the 1D Brillouin zone was used. The phonon calculations were performed with the method of finite differences.[27] We fully relaxed the atomic positions of both AGNRs and ZGNRs until the atomic forces of each atom were less than 0.01 eV/Å and minimized the total energy as function of lattice constant (refer to Tables I and II). We used a supercell approach with a $9\times9\times1$ supercell and the above parameters to calculate the phonon dispersion of graphene. These calculations resulted in a Γ-point frequency for the E_{2g} modes of 1622 cm^{-1}. This is slightly higher than the experimentally obtained graphene E_{2g} frequency of about 1580 cm^{-1}.[28] In order to achieve a better comparability between our calculated results and possible experimentally obtained results, e.g., by use of Raman spectroscopy, we scaled all calculated frequencies by a constant, such that the E_{2g} mode of our

calculated graphene phonon dispersion has the same frequency as the experimentally obtained value. The downscaled phonon dispersion of graphene is in very good agreement with experimentally obtained results[29,30] for graphite.

III. RESULTS AND DISCUSSION

Graphene nanoribbons have a large length to width ratio, which results in a quasi-1D crystal-like behavior and is expected to lead to confinement effects for the π orbital electrons perpendicular to the ribbon axis. It is therefore justified to regard the nanoribbons as infinitely long in our phonon calculations. Thus, the phonon wave vector in direction of the ribbon axis, $\mathbf{k}_{\parallel}$, is quasicontinuous. The ribbon edges however only allow standing waves perpendicular to the ribbon axis and thus induce the boundary condition

$$k_{\perp,n} \cdot w_{\text{ribbon}} = n \cdot \pi$$

on the phonon wave $f(r,t)=A \cdot e^{i(\mathbf{k}\cdot\mathbf{r}-\omega t)}$, leading to a quantized wave vector

$$k_{\perp,n} = \frac{\pi}{w_{\text{ribbon}}} \cdot n \tag{3}$$

with the order of vibration $n=0,\ldots,N-1$.

We expect therefore a vibrational behavior similar to that of an elastic sheet or a chain of N atoms with fixed or free ends, i.e., the appearance of fundamental vibrations and overtones. The phonon spectrum of an N-AGNR or N-ZGNR should comprise of six fundamental modes and $3 \cdot 2N-6 = 6(N-1)$ overtones. Therefore, in a given phonon spectrum, we should be able to assign $N-1$ overtone modes to each fundamental mode.

A. Armchair nanoribbons

Our calculations yield for each AGNR a Γ-point phonon spectrum consisting of $3m$ modes, with m the number of atoms per unit cell. The atomic displacements of these Γ-point modes can be classified into pure longitudinal (L), transverse (T), or out-of-plane (Z) modes. Each Γ-point phonon mode can be associated with one of three types which will be discussed separately: (1) C-H modes resulting from the passivation with hydrogen, (2) fundamental modes, or (3) overtones.

1. C-H modes

The four hydrogen atoms in the unit cell of AGNRs give 12 vibrational modes. These modes show large amplitudes of the hydrogen atoms in contrast to the almost negligibly small displacements of the carbon atoms. They can be grouped into six pairs of degenerate modes with different polarizations. Independent of the nanoribbon width, we find C-H modes at $\sim$750 cm^{-1}. These modes are bond-bending modes, where the hydrogen atoms move out of plane and the C-H bond length remains constant. The hydrogen atoms on a particular edge move in phase and perpendicularly to the C-H bond. Another pair of out-of-plane bond-bending C-H modes is found at a frequency of $\sim$880 cm^{-1}; again independent of the nanoribbon width. Here, the hydrogen atoms at the edge move out of phase. Similarly, there are two pairs of degenerate in-plane bond-bending modes, where the hydrogen atoms move perpendicular to the C-H bond. One pair with in-phase movement of the hydrogen atoms at an edge ($\sim$1100 cm^{-1}) and another pair, where the hydrogen displacements are out of phase ($\sim$1200 cm^{-1}). In addition, there are two pairs of stretching modes at $\sim$3100 cm^{-1} (in phase) and $\sim$3120 cm^{-1} (out of phase).

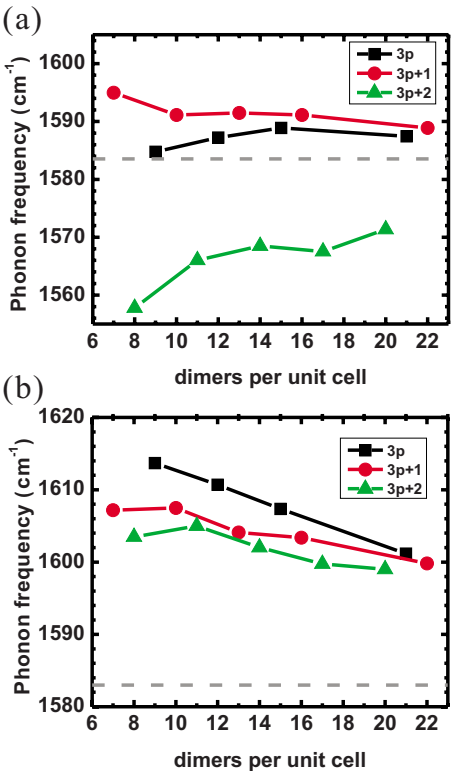

FIG. 2. (Color online) (a) Longitudinal-optical and (b) transverse-optical fundamental mode frequencies of armchair nanoribbons. Our calculated phonon frequencies were scaled by a constant factor to achieve a better compatibility of calculations and experimental values. The dashed line indicates the experimental E_{2g} frequency of graphene.

2. Fundamental modes

In any nanoribbon, a group of six modes can be found that are equivalent to the six Γ-point phonon modes of graphene with respect to the phonon eigenvectors. The two in-plane optical modes, in contrast to the graphene optical modes, are not found to be degenerate: the in-plane transverse-optical (TO) mode has a higher frequency than the in-plane longitudinal-optical (LO) mode for each of our studied AGNRs.

The frequencies of these modes are displayed in Fig. 2, together with the frequency of the experimental E_{2g} mode in graphene. According to Son *et al.*,[20] the nanoribbons can be classified into families $N=3p$, $N=3p+1$, and $N=3p+2$, with p a positive integer. The LO-TO splitting found for ribbons of the $N=3p$ family is about 29 cm^{-1} for the smallest investigated nanoribbon and about 14 cm^{-1} for the largest one. For the $N=3p+1$ family, we found a splitting of

12–14 cm^{-1} for all investigated nanoribbons. The $N=3p+2$ family displays a larger splitting. It is about 46 cm^{-1} for the 8-AGNR and decreases with increasing ribbon width to a value of about 27 cm^{-1} for a 20-AGNR. All these LO-TO splittings should be experimentally measurable. For the LO modes with $N=3p$ and $N=3p+1$ and the TO modes an increase in the frequency compared to graphene is found. As can be seen, the LO frequencies of the $(3p+2)$ nanoribbons are softened. This can be attributed to the small band gap in the quasimetallic $(3p+2)$ nanoribbons, which is smaller than 0.294 eV for $p>3$. This is similar to the LO phonon softening in metallic carbon nanotubes.[31,32] We assume that the same effect of strong electron-phonon coupling related to a Kohn anomaly takes place in quasimetallic GNR.[33] All modes converge toward the graphene frequency with increasing width.

3. Overtones

For each fundamental oscillation, we find $(N-1)$ overtones, where the fundamental displacement pattern is modified by an envelope forming a standing wave with $x=1,\ldots,N$ nodes. The vibrational behavior of these modes shows similarities to elastic sheets with free ends. The atomic displacement can be described by an enveloping cosine function

$$f_n = A_n \cos k_{\perp,n} x = A_n \cos \frac{\pi}{\lambda_{\perp,n}} x,$$

where n is the order of vibration, $k_{\perp,n}$, $\lambda_{\perp,n}$, and A_n refer to the wave number, the wavelength, and the amplitude of the nth order vibration. For the wave numbers hold the following relations:

$$k_{\perp,n} = \frac{2\pi}{\lambda_{\perp,n}}, \tag{4}$$

$$= \frac{\pi}{w_{\mathrm{AGNR}}} = \frac{2\pi}{(N-1)a_0} n. \tag{5}$$

The nodes do not have to coincide with carbon atom positions in the unit cell. Figure 3 shows the displacement patterns of a 7-AGNR. We characterize the phonon modes by their direction of vibration (transverse, longitudinal, and out of plane) and their nature (acoustic and optical) as n-L/T/ZA and n-L/T/ZO, with $n=$number of nodes.

B. AGNR modes in relation to graphene

Figure 4 shows the Brillouin zones of graphene, armchair nanoribbons, and zigzag nanoribbons. The hexagonal structure with high-symmetry points K and M represents the Brillouin zone of graphene with the distances $\overline{\Gamma K}=4\pi/3a_0$ and $\overline{\Gamma M}=2\pi/\sqrt{3}a_0$. As already discussed, the phonon vectors in nanoribbons are restricted by an edge-induced boundary condition, resulting in N quantized wave numbers $k_{\perp,n}$ along the ribbon width [Eq. (5)]. The component in axial direction however is unrestricted and not quantized. We find that the Brillouin zone of graphene nanoribbons consists of N equally

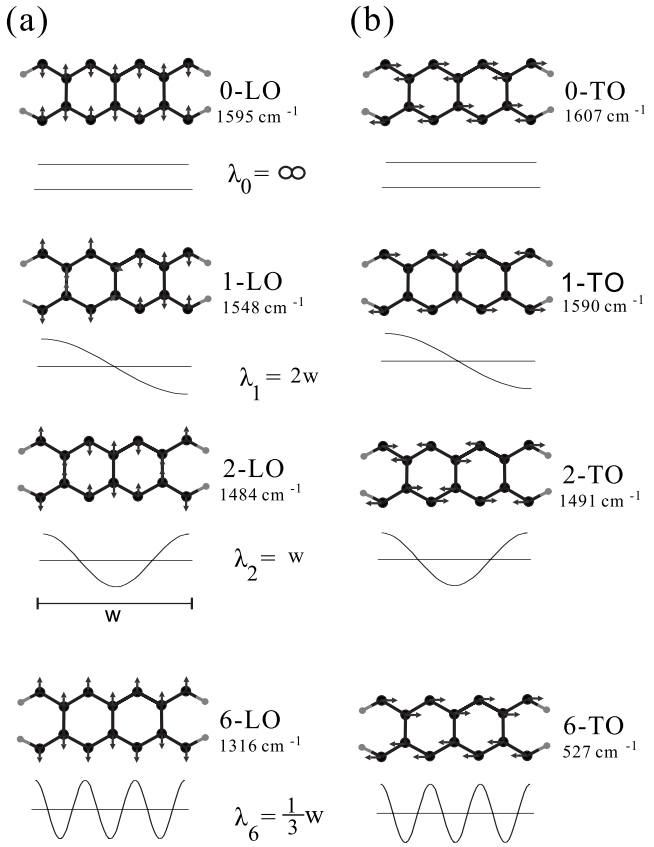

FIG. 3. (a) LO and (b) TO fundamental and overtone modes at the Γ point of a 7-AGNR. The arrows display the displacements of the atoms in the unit cell. The displacement strength is normalized to emphasize the node positions. For the n-L/TO, the eigenvectors of the atoms reverse n times 0-L/TO across the ribbon width. This is further clarified by the envelope curves. The wavelength of the vibrations is $\lambda=\frac{2}{n}w_{\mathrm{AGNR}}$.

spaced discrete lines, similar to the Brillouin zone of carbon nanotubes.[34] The line spacing for armchair nanoribbons is, from Eq. (5), $\Delta k_{\perp,n}=\frac{2\pi}{(N-1)a_0}$. The translation vector of an

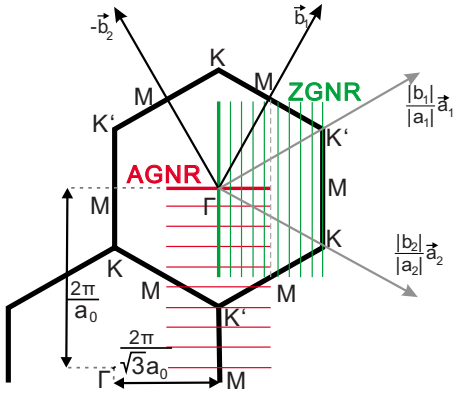

FIG. 4. (Color online) Brillouin zones of graphene, armchair (10-AGNR) and zigzag (10-ZGNR) nanoribbons. $\vec{a}_1$ and $\vec{a}_2$ are the lattice vectors of graphene, $\vec{b}_1$ and $\vec{b}_2$ are the reciprocal-lattice vectors. Note that the Brillouin zone of ZGNRs is idealized; in actual nanoribbons it reaches the K-M-K' line only in the limit of large nanoribbons, see discussion in Sec. III C.

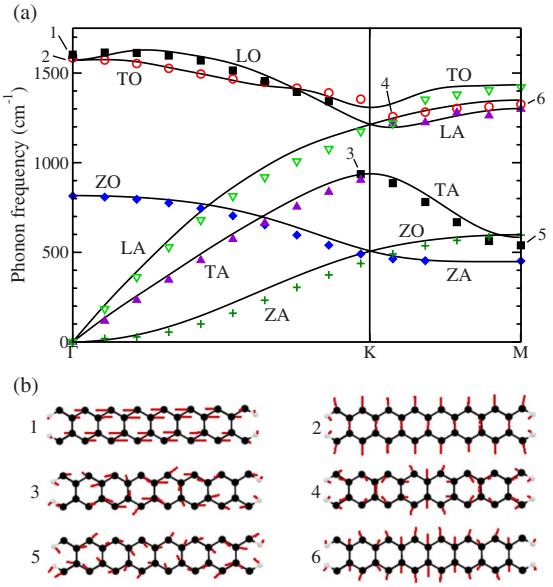

FIG. 5. (Color online) (a) Mapping of TO (filled squares), LO (circles), ZO (filled diamonds), TA (open triangles), LA (filled triangles), ZA (pluses) fundamental, and overtone frequencies of an 15-AGNR onto our calculated phonon dispersion of graphene (solid lines). Longitudinal ribbon modes correspond to transverse graphene modes. (b) Eigenvectors of selected ribbon TO and LO frequencies in the Γ*KM* direction. The corresponding modes are indicated in (a).

armchair nanoribbon is given by $\vec{a}_{\mathrm{AGNR}}=\vec{a}_1+\vec{a}_2$, i.e., the axial direction of armchair nanoribbons corresponds to the Γ*M* direction in graphene. The direction perpendicular to the ribbon axis corresponds to the Γ*KM* direction. The AGNR Γ-point overtone vibrations therefore correspond to vibrations in the Γ*KM* direction.

Aside from the existence of hydrogen passivation and the difference of C-C bond lengths between carbon atoms at the nanoribbon edges and between atoms in the middle of the nanoribbon due to edge effects, the unit cell of a graphene nanoribbon is very similar to a supercell of graphene unit cells. For this reason, we expect that zonefolding of the phonon dispersion of graphene yields a reasonable approximation of the phonon dispersions of nanoribbons, especially for larger nanoribbons, where edge effects should have a smaller influence on the phonon dispersions. Therefore, we will show how to "unfold" the nanoribbon's Brillouin zone onto that of a graphene sheet, where the Γ-point fundamental and overtone modes of an AGNR reproduce the graphene modes along the Γ*KM* direction. For the overtone of the highest order, i.e., $n=N-1$, we find from Eq. (5)

$$k_{\perp,N-1}=\frac{2(N-1)\pi}{(N-1)a_0}=\frac{2\pi}{a_0}.$$

As can be seen in Fig. 4, $|\overline{\Gamma KM}|=2\pi/a_0$, thus it should be possible to reproduce the whole Γ*KM* dispersion of graphene by nanoribbon Γ-point overtones. Figure 5 shows a mapping of the resulting pairs $(k_{\perp,n},\omega_n)$ of AGNR Γ-point phonon modes onto the phonon dispersion of graphene. As we defined the longitudinal and transverse directions with respect to the ribbon axis, the *n*th overtone of a longitudinal ribbon mode corresponds to a transverse phonon at wave vector $k_{\perp,n}$ in graphene and vice versa.

The overtones of one respective ribbon fundamental mode reproduce different phonon branches of graphene in Γ*K* and *KM* directions. For example, the ribbon TO frequencies reproduce the graphene LO branch in the Γ*K* direction but then switch to the graphene TA branch beyond the *K* point. The reason for this lies in the strict mode classification applied to the nanoribbons. We can also understand the branch switching from the Brillouin zone of graphene (see Fig. 4): going along Γ*K* and then along *KM*, the direction of the wave vector changes by 120°, if one continues to stay in the first Brillouin zone of graphene. Moreover, it is well known that close to the *K* point the phonon modes loose their purely longitudinal or transverse character. Figure 5(b) shows the phonon eigenvectors of different overtones of the nanoribbon modes. It is clearly seen that the overtones near the graphene *K* point have a mixed character with displacements in different directions [see panels 3 and 4 in Fig. 5(b)]. In total, only small deviations between the calculated graphene dispersion and the zonefolded nanoribbon frequencies are found. It is expected that ribbon frequencies converge toward the graphene dispersion with increasing ribbon width, a result which we find confirmed. The root-mean-square deviation between graphene LO branch and their corresponding ribbon modes decreases from 59 cm^{-1} (7-AGNR) to 31.5 cm^{-1} (14-AGNR).

In general, the overtones reproduce the graphene phonon dispersion fairly well, especially for longer wavelengths, i.e., near the Γ point. The agreement weakens a little for wavelengths near the edge of the graphene Brillouin zone, the nanoribbon's overtones slightly deviate from the calculated graphene dispersion branches, as seen in Fig. 5(a). It is conceivable that this slight deviation is due to effects of the finite structure perpendicular to the nanoribbon axis and the resulting changes in C-C bond lengths at the nanoribbon edges. Further, it is apparent from our mapping that the overtones do not reproduce the special phonon structure near the *K* point. There, the TO mode of graphene displays a noticeable drop in frequency due to a Kohn anomaly,[21,30,33] i.e., a strong electron-phonon coupling. As visible in Fig. 6(a), the nanoribbon overtones show a poorer reproduction of this drop of frequency in the surrounding of the graphene *K* point. This is understandable because of the semiconducting nature of the investigated nanoribbons, which would prevent the formation of Kohn anomalies. In this case, armchair nanoribbons with smaller band gaps should reproduce the graphene dispersion near the *K* point better than AGNRs with larger gaps. Indeed, our calculations suggest that the quasimetallic AGNRs of the $N=3p+2$ family, which have very small band gaps, give slightly better results than the ribbons of the other families. As mentioned above, the nanoribbon modes change their character from longitudinal to transverse direction and vice versa when crossing the *K* point. In particular, the displacement vectors of the ribbon LO between *K* and *M* show strong similarities with the LA branch in graphene. Correspondingly, the frequencies agree well with the LA branch [Fig. 6(a)]. Similarly, the nanoribbon TO modes switch in characteristics to TA eigenvectors

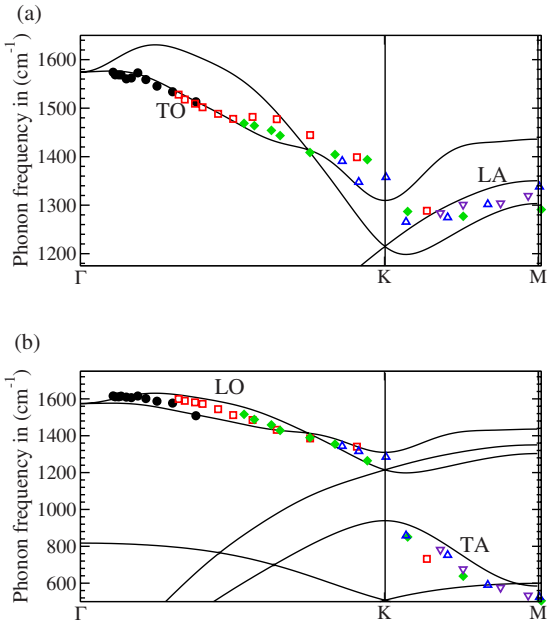

FIG. 6. (Color online) (a) n-LO and (b) n-TO overtones of N-AGNRs with $N=5-15$ and $n=1$ (filled circles), $n=3$ (empty squares), $n=5$ (filled diamonds), $n=8$ (empty triangles), and $n=11$ (crosses). Solid black lines are the calculated graphene modes as in Fig. 5.

when crossing the K point in M direction [Fig. 6(b)]. We find thus that the overtones of the nanoribbons can be well mapped onto the graphene dispersion when including the character of their eigenvectors. In graphene, the overtones correspond to different branches in the Γ-K and K-M parts of the Brillouin zone.

Overall we encountered difficulties in characterizing modes close to the graphene K point. The characteristic overbending of the graphene LO mode due to a Kohn anomaly at the Γ point is found by zone folding of the ribbon modes, too, for nanoribbons of sufficient width ($N>8$). However, the observed overbending is considerably smaller than the one in the calculated graphene dispersion.

C. Zigzag nanoribbons

Recent studies show that the ground state of zigzag nanoribbons displays antiferromagnetically ordered spin states.[10,15,35] Calculations using spin polarization predict the opening of a band gap for the otherwise metallic ZGNRs and half-metallic behavior when an electric field is applied due to the opposite behavior of different spin directions in electric fields.[15] We analyzed the phonon spectra of ZGNRs for effects due to the band-gap opening by generating a pseudopotential including spin polarization with using exactly the same cutoff radii as the pseudopotentials we used for calculations neglecting spin polarization. We find excellent agreement with the results of Son *et al.*[15] regarding the band gap. While the spin-polarization effects are vital for the electronic properties, we observe only small effects on the vibrational frequencies. Our calculated Γ-point frequencies differ by just up to 8 cm^{-1} from calculations neglecting spin polarization. For this reason, we did not include spin polarization in the following phonon calculations.

In order to study the vibrational behavior of zigzag nanoribbons, we carried out calculations on N-ZGNRs with $N=3\cdots14$ and performed the same rescaling of the calculated frequencies as was done for AGNRs. A distinction of the Γ-point phonons in fundamental modes, overtones, and C-H modes (only doubly degenerate pairs at $\sim$750 cm^{-1}, $\sim$1100 cm^{-1}, and $\sim$3100 cm^{-1} are found) is performed as for the armchair nanoribbons. The direction perpendicular to the ribbon axis reproduced by the mapping corresponds to the ΓM direction of graphene, see Fig. 4. The wavelengths of the vibrations of equivalent carbon atoms over the nanoribbon width can be described by

$$\lambda_n = \frac{2}{n} w_{\mathrm{ZGNR}}. \tag{6}$$

By Eqs. (2), (4), and (6), we calculate a line spacing of

$$\Delta k_\perp = \frac{2\pi}{\lambda_{n+1}} - \frac{2\pi}{\lambda_n} = \frac{2\pi}{\sqrt{3}(N-1)a_0}.$$

The overtone of highest order, $k_{\perp,N-1}$, is then

$$k_{\perp,N-1} = \Delta k_\perp (N-1) = \frac{2\pi}{\sqrt{3}(N-1)a_0}(N-1) = \frac{2\pi}{\sqrt{3}a_0}.$$

This is equal to the graphene Γ-M distance, as $|\overline{\Gamma M}| = \frac{2\pi}{\sqrt{3}a_0}$. Therefore, we can, in theory, reproduce the whole $\overline{\Gamma M}$ of the graphene dispersion by unfolding the Γ-point phonons of ZGNRs of finite width. On the other hand, we determined the wavelengths of the overtones of our investigated ribbons by fitting a cosine function to the respective displacement patterns and compared them to the theoretically expected values. For small nanoribbons, we found considerable deviations between the wavelength of the lattice vibration of graphene at the M point and the smallest wavelength that the atomic displacements of the nanoribbon can describe, i.e., the wavelengths of the highest order overtones. Thus, the mapping of the Brillouin zone of small nanoribbons cannot reproduce the whole ΓM direction, as $k_{\perp,N-1} < k_{M\ \mathrm{point}} = \frac{2\pi}{\sqrt{3}a_0}$. However, these smallest wavelengths quickly converge toward the graphene M-point wavelength with increasing ribbon width. We performed mappings of the phonon modes of ZGNRs of various widths onto the graphene phonon dispersion in the ΓM direction (Fig. 7). Again, unfolding the ribbon overtones onto the Brillouin zone of graphene shows good agreement, which improves for increasing ribbon width. The overtones of highest order of the optical modes of small nanoribbons appear to be clinched due to the mentioned deviations of fitted and theoretically predicted wavelength. The acoustical modes, however, display a great agreement of nanoribbon overtones and graphene dispersion. The ZGNR fundamental mode frequencies correspond to the six Γ-point frequencies of graphene. For ZGNRs we see, in contrast to AGNRs, a clear separation between the frequencies of in-plane acoustic and optical phonon modes. The in-plane acoustic modes are found in a frequency interval of $0-1300$ cm^{-1}, the (in-plane) optical modes lie between 1300

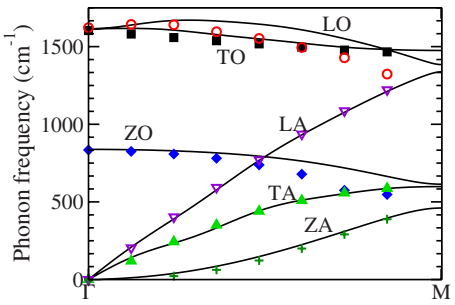

FIG. 7. (Color online) Mapping of ribbon LO (filled squares), TO (circles), ZO (filled diamonds), TA (down triangles), LA (filled-up triangles), ZA (crosses) fundamental, and overtone frequencies of an 8-ZGNR onto the calculated phonon dispersion of graphene (solid lines). $k_{\perp,N-1}$ does not reach the graphene M point, as for ZGNRs of small width, the wavelengths obtained by fitting the displacement pattern of the calculated phonons are larger than the theoretically predicted ideal values.

and 1600 cm^{-1} and are straightforward to classify as all of them are of pure longitudinal or transverse nature. The displacement pattern of ZGNRs shows no apparent mixing of modes, as found for AGNRs. As mentioned in Sec. III B, the mixing of modes in AGNRs occurs due to the symmetries at the graphene K point. However, there's no comparable point in the ΓM direction, which is reproduced by the mapping of the ZGNR Brillouin zones onto the one of graphene.

Figure 8 shows a comparison of in-plane phonon mode frequencies of N-ZGNRs with $N=2\cdots14$. As was found for AGNRs, the 0-LO of the ribbon converges toward the graphene LO for increasing ribbon width. A similar behavior is found for the longitudinal-optical overtones. For the frequency of the 0-TO, a nonmonotonic dependence on the ribbon width is observed. The calculated frequencies of the transverse-optical overtones of low order are higher than those of the 0-TO. Similarly as for the AGNRs we thus find for ZGNR a (small) overbending for the graphene LO mode with our zone-folding method, at least for sufficiently large ribbon widths. The acoustic overtones of both longitudinal and transverse nature display an inversely proportional width dependence. In case of transverse overtones, this width dependence is well described by $\omega_{ac} \propto N^{-1}$. Longitudinal acoustic overtones, however, show a considerably weakening width dependence with increasing vibrational order, as can be seen in Fig. 8(b).

Finally, we calculated the phonon dispersions over the whole Brillouin zone of various small nanoribbons by means of a supercell approach. We used a supercell of nine unit cells along the nanoribbon axis. Figure 9(a) shows the dis-

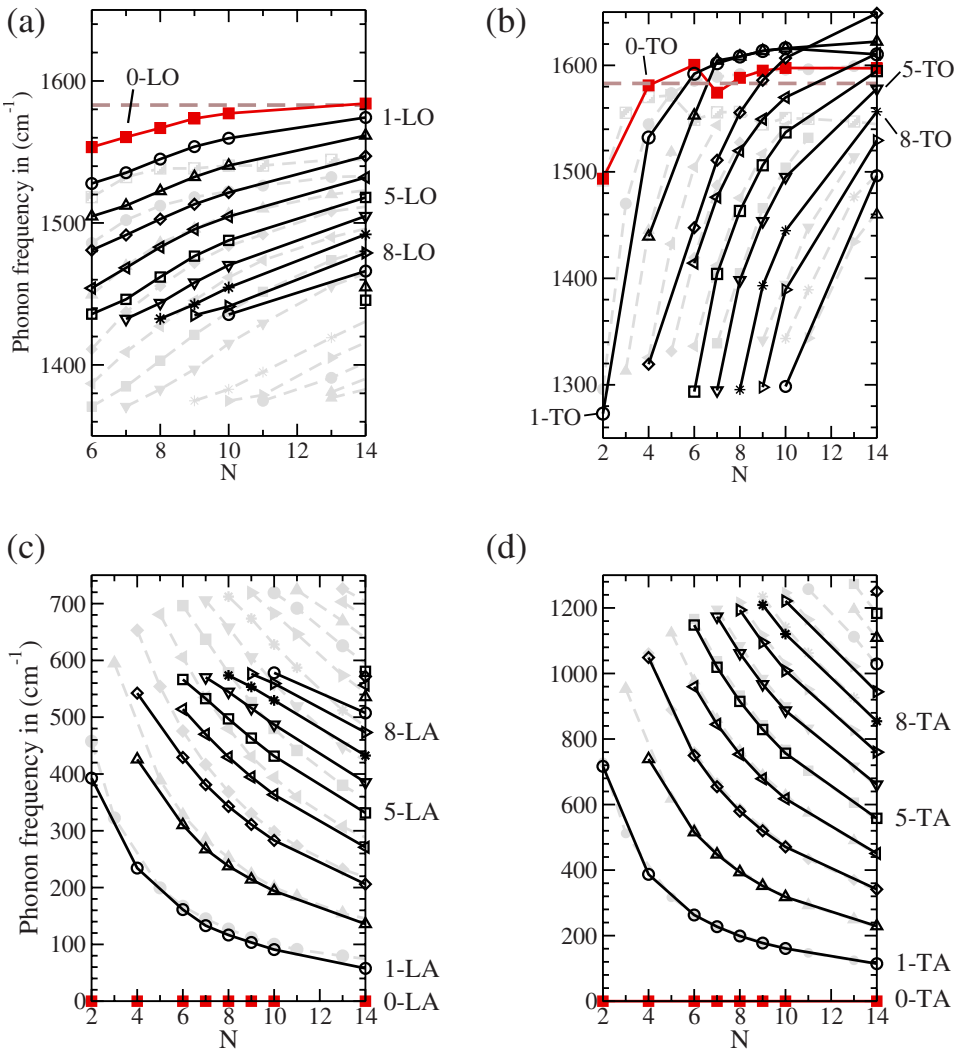

FIG. 8. (Color online) [(a) and (c)] Calculated longitudinal and [(b) and (d)]transverse Γ-point frequencies of the ZGNR in dependence of nanoribbon width. Filled (red) squares are fundamental oscillations and empty symbols are overtones. Solid black lines connect overtones of equal order n for different ribbons. Filled gray symbols connected with dashed lines show the results of calculations of Yamada *et al.* (Ref. 23) for comparison. The experimentally determined E_{2g} mode frequency of 1580 cm^{-1} is indicated by thick (brown) dashed lines.

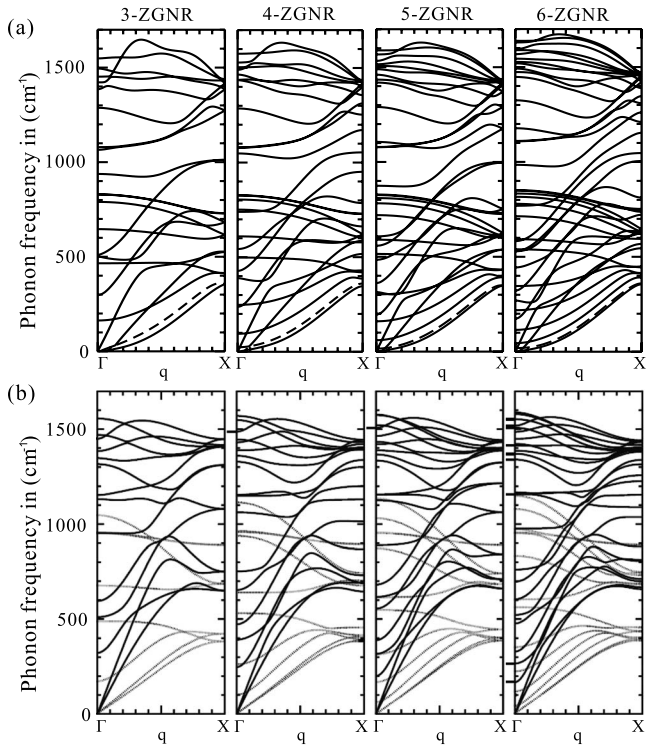

FIG. 9. Phonon dispersions of hydrogenated *N*-ZGNRs with $N=3-6$ obtained by (a) DFT and (b) MO/8 calculations done by Yamada *et al.* (Ref. 23). The dashed lines in (a) indicate the fourth acoustic mode, typical for 1D crystals. Dashed lines in (b) are out-of-plane vibrations.

persions of *N*-ZGNR with $N=3-6$. As can be seen, the dispersions feature the characteristic fourth acoustic mode of 1D structures, which is a rotational mode around the *z* axis. The displacement pattern of this mode at the Γ point corresponds to the displacement pattern of the mode we classify as 1-ZA. However, the 1-ZA in our calculations has a frequency $\omega_{1ZA}=5-20$ cm^{-1}, which we believe results from the presence of the hydrogen passivation and possibly also from numerical errors. The two out-of-plane acoustic modes converge swiftly for increasing ribbon widths, being noticeably separated for the 3-ZGNR but almost degenerate for the 6-ZGNR, closely resembling the ZA mode of graphene. An interesting fact was found for the phonon modes at the *X* point: In armchair nanotubes the phonon modes are pairwise degenerate, i.e $6(n-1)$ phonon modes in (n,n) CNTs with odd n and all modes in (n,n) CNTs with even n, at the *X* point due to symmetry.[35] Therefore, we might expect $6(N-1)$ pairwise degenerate and six nondegenerate modes in *N*-ZGNR with odd *N*. Similarly, all phonon modes of *N*-ZGNRs with even *N* should be pairwise degenerate. However, we do not find a similar degeneracy for the zigzag nanoribbon dispersions we studied so far. In fact, the calculated phonon spectra of *N*-ZGNR with odd *N* consist solely of modes that are pairwise degenerate at the *X* point. In contrast, the phonon modes of *N*-ZGNR with even *N* are largely nondegenerate at the edge of the Brillouin zone.

We want to compare our results with previous calculations by Yamada *et al.*[23] They applied a molecular orbital method, which uses force fields based on Hückel theory, i.e., a semiempirical approach.[36] This approach was shown to be efficient for calculating the vibrational properties of polycyclic aromatic hydrocarbons such as graphene. In this approach, the topology of the structures of interest is fixed consisting of hexagons with C-C bond lengths of 1.39 Å and C-H bond lengths of 1.048 Å. As can be seen in Figs. 8 and 9(b), we find general agreement but some deviations, in particular, for the longitudinal modes. We suggest the geometry relaxation that we performed in our calculations to be the source of these deviations.

IV. CONCLUSION

We investigated the vibrational properties of graphene nanoribbons with density-functional theory. We showed that the Γ-point phonons of graphene nanoribbons with armchair- and zigzag-type edges can be interpreted as six fundamental oscillations and their overtones, which show a characteristic nanoribbon width dependence. We further found a family dependence for the fundamental modes of AGNRs, which is in correspondence to the known family behavior of the band gaps of AGNRs.[20] The longitudinal-optical and transverse-optical modes in our calculations feature a noticeable splitting of up to 46 cm^{-1} and should be experimentally measurable, e.g., by means of Raman spectroscopy, which would be an interesting task for future works. We demonstrated that the Γ-point phonon frequencies of nanoribbons can be mapped onto the phonon dispersion of graphene, i.e., to an "unfolding" of the nanoribbons' Brillouin zone onto that of graphene. The edge magnetization and the resulting opening of a band gap in zigzag nanoribbons has only a small influence on the phonon spectra. The behavior of overtones and fundamental modes for nanoribbons of increasing width was studied and a comparison of our results for ZGNRs with past studies performed.

ACKNOWLEDGMENTS

This work was supported in part by the Cluster of Excellence "Unifying Concepts in Catalysis" coordinated by the TU Berlin and funded by DFG.

[1] K. S. Novoselov, A. K. Geim, S. V. Morozov, D. Jiang, Y. Zhang, S. V. Dubonos, I. V. Grigorieva, and A. A. Firsov, Science **306**, 666 (2004).

[2] Y. Zhang, Y.-W. Tan, H. L. Stormer, and P. Kim, Nature (London) **438**, 201 (2005).

[3] C. Berger, Z. Song, X. Li, X. Wu, C. N. Nate Brown, D. Mayou, T. Li, J. Hass, A. N. Marchenkov, E. H. Conrad, P. N. First, and W. A. de Heer, Science **312**, 1191 (2006).

[4] K. S. Novoselov, Z. Jiang, Y. Zhang, S. V. Morozov, H. L. Stormer, U. Zeitler, J. C. Maan, G. S. Boebinger, P. Ki, and A. K. Geim, Science **315**, 1379 (2007).
[5] M. Y. Han, B. Özyilmaz, Y. Zhang, and P. Kim, Phys. Rev. Lett. **98**, 206805 (2007).
[6] X. Li, X. Wang, L. Zhang, S. Lee, and H. Dai, Science **319**, 1229 (2008).
[7] D. Kosynkin, A. Higginbotham, A. Sinitskii, J. Lomeda, A. Dimiev, B. Price, and J. Tour, Nature (London) **458**, 872 (2009).
[8] L. Jiao, L. Zhang, X. Wang, G. Diankov, and H. Dai, Nature (London) **458**, 877 (2009).
[9] A. Cano-Marquez, F. Rodriguez-Macias, J. Campos-Delgado, C. Espinosa-Gonzalez, F. Tristan-Lopez, D. Ramirez-Gonzalez, D. Cullen, D. Smith, M. Terrones, and Y. Vega-Cantu, Nano Lett. **9**, 1527 (2009).
[10] M. Fujita, K. Wakabayashi, K. Nakada, and K. Kusakabe, J. Phys. Soc. Jpn. **65**, 1920 (1996).
[11] K. Wakabayashi, M. Sigrist, and M. Fujita, J. Phys. Soc. Jpn. **67**, 2089 (1998).
[12] K. Wakabayashi, M. Fujita, H. Ajiki, and M. Sigrist, Phys. Rev. B **59**, 8271 (1999).
[13] K. Kusakabe and M. Maruyama, Phys. Rev. B **67**, 092406 (2003).
[14] A. Yamashiro, Y. Shimoi, K. Harigaya, and K. Wakabayashi, Phys. Rev. B **68**, 193410 (2003).
[15] Y.-W. Son, M. L. Cohen, and S. Louie, Nature (London) **444**, 347 (2006).
[16] H. Lee, Y.-W. Son, N. Park, S. Han, and J. Yu, Phys. Rev. B **72**, 174431 (2005).
[17] A. V. Nikolaev, A. V. Bibikov, A. V. Avdeenkov, I. V. Bodrenko, and E. V. Tkalya, Phys. Rev. B **79**, 045418 (2009).
[18] M. Ezawa, Phys. Rev. B **73**, 045432 (2006).
[19] V. Barone, O. Hod, and G. Scuseria, Nano Lett. **6**, 2748 (2006).
[20] Y.-W. Son, M. L. Cohen, and S. G. Louie, Phys. Rev. Lett. **97**, 216803 (2006).
[21] S. Pisana, M. Lazzeri, C. Casiraghi, K. S. Novoselov, A. K. Geim, A. C. Ferrari, and F. Mauri, Nature Mater. **6**, 198 (2007).
[22] M. Yamada, Y. Yamakita, and K. Ohno, Phys. Rev. B **77**, 054302 (2008).
[23] J. P. Perdew and A. Zunger, Phys. Rev. B **23**, 5048 (1981).
[24] N. Troullier and J. L. Martins, Phys. Rev. B **43**, 1993 (1991).
[25] J. M. Soler, E. Artacho, J. Gale, A. Garcia, J. Junquera, and P. Ordejoń, J. Phys.: Condens. Matter **14**, 2745 (2002).
[26] P. Ordejón, E. Artacho, and J. M. Soler, Phys. Rev. B **53**, R10441 (1996).
[27] M. T. Yin and M. L. Cohen, Phys. Rev. B **26**, 3259 (1982).
[28] A. C. Ferrari, J. C. Meyer, V. Scardaci, C. Casiraghi, M. Lazzeri, F. Mauri, S. Piscanec, D. Jiang, K. S. Novoselov, S. Roth, and A. K. Geim, Phys. Rev. Lett. **97**, 187401 (2006).
[29] M. Mohr, J. Maultzsch, E. Dobardžić, S. Reich, I. Milošević, M. Damnjanović, A. Bosak, M. Krisch, and C. Thomsen, Phys. Rev. B **76**, 035439 (2007).
[30] J. Maultzsch, S. Reich, C. Thomsen, H. Requardt, and P. Ordejón, Phys. Rev. Lett. **92**, 075501 (2004).
[31] O. Dubay, G. Kresse, and H. Kuzmany, Phys. Rev. Lett. **88**, 235506 (2002).
[32] S. Piscanec, M. Lazzeri, J. Robertson, A. C. Ferrari, and F. Mauri, Phys. Rev. B **75**, 035427 (2007).
[33] S. Piscanec, M. Lazzeri, F. Mauri, A. C. Ferrari, and J. Robertson, Phys. Rev. Lett. **93**, 185503 (2004).
[34] S. Reich, C. Thomsen, and J. Maultzsch, *Carbon Nanotubes: Basic Concepts and Physical Properties* (Wiley-VCH, Berlin, 2004).
[35] S. Okada and A. Oshiyama, Phys. Rev. Lett. **87**, 146803 (2001).
[36] K. Ohno, R. Takahashi, M. Yamada, and Y. Isogai, Internet Electron. J. Mol. Des. **1**, 636 (2002).